Effect of Decarboxylation on the Photoinitiation Behavior of Nitro-Carbazole based Oxime Esters

Shaohui Liu[1,2], Nicolas Giacoletto[3], Michael Schmitt[1,2], Malek Nechab[3], Bernadette Graff[1,2], Fabrice Morlet-Savary[1,2], Pu Xiao[4]*, Frédéric Dumur[3]*, Jacques Lalevée[1,2]*

[1]Université de Haute-Alsace, CNRS, IS2M UMR 7361, F-68100 Mulhouse, France
[2]Université de Strasbourg, France
[3]Aix Marseille Univ, CNRS, ICR UMR 7273, F-13397 Marseille, France
[4]Research School of Chemistry, Australian National University, Canberra, ACT 2601, Australia

*Corresponding authors: pu.xiao@anu.edu.au; frederic.dumur@univ-amu.fr; jacques.lalevee@uha.fr

ABSTRACT: A series of fifty oxime esters photoinitiators (PIs) bearing various substituents were designed and synthesized for this study (48 of them were never synthesized before and only B1 and B10 were reported). Due to the presence of a nitro group onto carbazole, good light absorption properties in the visible range were evidenced for these PIs. Some structures exhibited better photoinitiation abilities than diphenyl(2,4,6-trimethylbenzoyl)phosphine oxide (TPO) upon exposure to LED@405 nm. 3D printing experiments were successfully carried out using the most reactive oxime ester PI. Thermal initiation behaviors of several oxime esters were also studied through differential scanning calorimetry (DSC). The proposed photochemical mechanism was investigated by steady state photolysis, determination of the enthalpy of cleavage process and electron spin resonance - spin trapping experiments. Interestingly, the PIs with methyl substituent on oxime ester group have the best photoinitiation performance. Substituent effects were investigated through molecular orbitals calculations, the detection of CO_2 and the investigation of the generated free radicals. The results demonstrate that the substituents on the oxime ester group exert major effects on the photoinitiation ability via decarboxylation reaction.
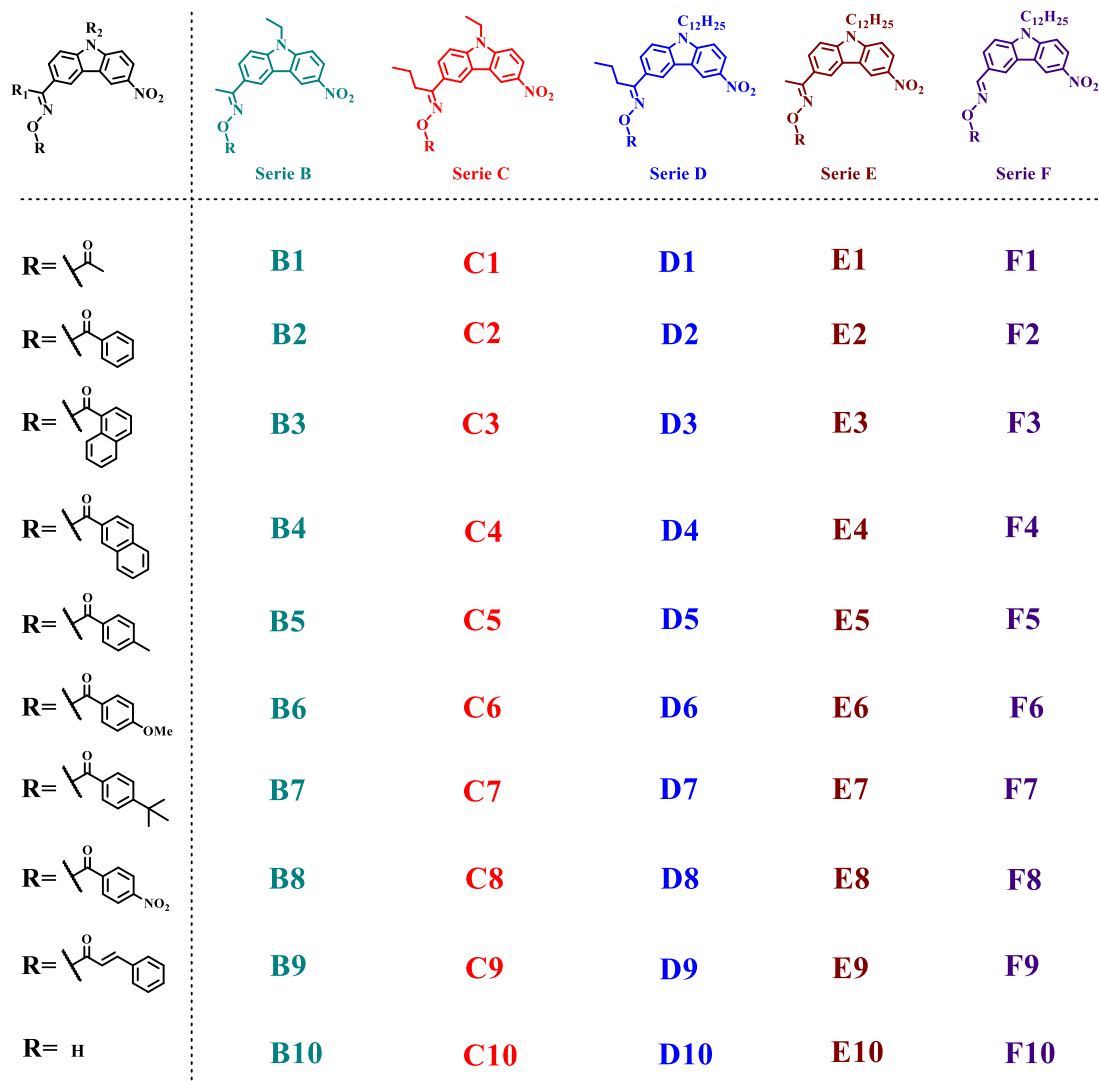
INTRODUCTION

Photopolymerization technology has been developing steadily benefiting from the characteristics of spatial and temporal controllability, environmental protection, and efficient process.[1-6] Light-emitting diodes (LEDs) have been used as irradiation sources in photopolymerization increasingly due to their higher safety, lower energy consumption and longer emission wavelength than the conventional mercury lamp.[7] Nowadays, LEDs are almost the primary choice to carry out photopolymerization experiments. Because of the narrow emission band, a considerable part of commercial photoinitiators (PIs) can be initiated effectively under UV light sources rather than near UV or visible LEDs.[8-10] Increasing numbers of two- or three-component photoinitiating systems whose light absorption spectra can match with the emission of LEDs have been designed and developed,[11, 12] while the electron transfer efficiency in multi-step initiating processes and the viscous resins for the photoinitiating systems are the drawbacks to face.[13] Therefore, it is desirable to develop one-component Type I PIs which can cleavage directly upon exposure of LEDs to generate free radicals for photopolymerization reactions.

Currently, only a few Type I PIs including α-amino ketones and phosphine-oxides are suitable with near UV and visible LEDs.[14, 15] Oxime esters (OXE) are well-known for their high reactivities in free radical photopolymerization as Type I PI.[16-21] Normally, the N−O bond in OXE structure cleave under light irradiation to generate iminyl and acyloxy radicals. Next, acyloxy radicals undergo a decarboxylation reaction that produces CO_2 and another active radical which is capable of initiating the free radical polymerization.[22-24] Two commercial OXEs O-benzoyl- α -oxooxime (OXE 01) and O-acetyloxime (OXE 02) are used to manufacture thick films in color filter resists.[25] However, the absorption bands of OXE 01 and OXE 02 are located in the UV range, resulting in bad performances upon exposure to near UV or visible LEDs.[25, 26] Hence, it is interesting to design novel OXEs which exhibit longer absorption wavelengths to match the LEDs emissions.

In our previous work, three OXEs based on nitro-carbazole chromophore were studied.[27] Among them, the PI OXE-M where methyl substituent is attached on the terminal moiety of oxime ester demonstrated higher photoinitiation ability than the PI OXE-P where phenyl substituent is attached on the terminal moiety of oxime ester. Some OXEs were also reported by our group including triphenylamine-based and coumarin-based OXEs where the structures with the methyl substituent attached on the terminal moiety of oxime ester were also more efficient than the structures with the phenyl substituent attached on the terminal moiety of oxime ester.[28, 29] The reason was ascribed to the favorable enthalpy change of the decarboxylation reaction for acetoxy.[29] In addition, the same phenomenon is also reported by other literatures. Stilbene-based, carbazole-coumarin-based and phenylthioether thiophene-based oxime esters all demonstrated the same behavior where the PIs with the methyl substituent had better performance than that with the phenyl substituent.[30-32] Those literatures tend to attribute the results to the competitive cage recombination of the phenyl radical with its homolog.

To clarify the chemical structures/photoinitiation ability relationship of oxime ester-based PISs, five series of oxime ester derivatives with different substituents were designed for this study. The chemical structures of OXE PIs are illustrated in Scheme 1. OXEs were divided into five series, representing a total of fifty molecules. Series B, Series C, Series D, Series E and Series F are discriminated by the substituents R_1 and R_2. Meanwhile, each nitro-carbazole is combined with the different substituent R on oxime group. R, R_1 and R_2 are designed to investigate the substituent effects on the photoinitiation ability.

Scheme 1. Chemical structures of the fifty investigated OXEs.

R=	Serie B	Serie C	Serie D	Serie E	Serie F
(acetyl)	B1	C1	D1	E1	F1
(benzoyl)	B2	C2	D2	E2	F2
(1-naphthoyl)	B3	C3	D3	E3	F3
(2-naphthoyl)	B4	C4	D4	E4	F4
(4-methylbenzoyl)	B5	C5	D5	E5	F5
(4-OMe benzoyl)	B6	C6	D6	E6	F6
(4-tert-butylbenzoyl)	B7	C7	D7	E7	F7
(4-NO_2 benzoyl)	B8	C8	D8	E8	F8
(cinnamoyl)	B9	C9	D9	E9	F9
R= H	B10	C10	D10	E10	F10

EXPERIMENTAL SECTION

Materials

The monomer for free radical photopolymerization i.e. trimethylolpropane triacrylate (TMPTA) was obtained from Sartomer (France). Diphenyl(2,4,6-trimethylbenzoyl)phosphine oxide (TPO) was purchased from Lambson Ltd (United Kingdom). The free radical trapping agent i.e. phenyl-*N-tert*-butylnitrone (PBN) was obtained from TCI-Europe (Paris, France). The colloidal silica suspension (LUDOX® AS 30, 30 wt% suspension in H_2O) was obtained from Sigma-Aldrich.

UV-visible absorption spectra

UV-visible absorption spectra of PIs in acetonitrile were obtained by JASCO V730 spectrometer. Steady state photolysis of the PIs was carried out upon exposure to LED@405 nm. UV-visible spectra of PI at different irradiation times were measured by mean of the JASCO V730 spectrometer. The concentration of PIs was 5×10^{-5} M.

Photopolymerization

Photopolymerization kinetics of TMPTA were evaluated by Real-Time Fourier Transformed Infrared Spectroscopy (RT-FTIR) JASCO FTIR-4100. In order to avoid the O_2 inhibition, the resin was put in laminate between two polypropylene films with a thickness ~25 μm. The C=C characteristic peak area of TMPTA was selected from 1589 cm^{-1} to 1665 cm^{-1}. For the thick samples (1.4 mm), the resin was added into a plastic mould and the characteristic peak area was from 6105 cm^{-1} to 6221 cm^{-1}. The infrared spectra of TMPTA during irradiation could be recorded by RT-FTIR and the conversion of acrylate functions of TMPTA was obtained by the equation:

$$FC(\%) = \frac{A_0 - A_t}{A_0} \times 100\%$$

where FC is the final function conversion; A_0 is the proportion of the peak area at 0 s; A_t is the proportion of the peak area at t s. The PIs (2×10^{-5} mol/g TMPTA) and monomers were mixed and stirred in the dark for 24 h. Polymerization experiments were carried out using the LED@405 nm with the light intensity ~110 mW·cm^{-2}.

Fluorescence spectra and fluorescence lifetime

Fluorescence spectra of the PIs in acetonitrile (5×10^{-5} M) were measured on a JASCO FP-750 spectrofluorometer. Fluorescence excited state lifetimes were measured by HORIBA PPD-850 detector. The excitation wavelength was 367 nm and the pulse duration was shorter than 1.4 ns. The impulse response function (IRF) of the apparatus was evaluated through the colloidal silica suspension LUDOX®.

Electron spin resonance - spin trapping (ESR-ST)

Free radicals were tested through ESR-ST experiments by an X-band spectrometer (Bruker EMX-Plus). The free radical trapping agent was phenyl-*N-tert*-butylnitrone (PBN). Concentration of the PIs in *tert*-butylbenzene was 10^{-4} M and the experiments were carried out at room temperature upon exposure to LED@405 nm. In addition, the ESR spectra simulations could be obtained using the PEST WINSIM program.

3D printing

Direct laser write (DLW) experiments were carried out using a laser diode@405 nm (Thorlabs, UK). Intensity of the laser was 110 mW and the spot size was ~50 μm. The resin containing 1 wt% PI in TMPTA was irradiated under air to obtain the pattern which was observed through the numerical optical microscope (OLYMPUS DSX-HRSU). The 3D printer PHOTON S based on LCD screen @405 nm was obtained from Anycubic (China). The layer thickness was 0.02 mm and the exposure time was 20 s.

Thermal initiation behavior

The thermal initiation behavior of OXEs (1 wt%) in TMPTA was performed through differential scanning calorimetry (DSC) by heating (10 °C/min) from 20 to 250 °C under nitrogen using a Mettler Toledo DSC. The heat release of acrylate double bond is 78.61 kJ/mol in polymerization, so that the function conversion of TMPTA in thermal polymerization can be calculated (FC = (heat released/g)/ 795.9).[33]

Computational procedure

Triplet state energy (E_T) and N−O bond energy (N−O BDE) of OXEs were calculated with the density functional theory at the UB3LYP/6-31G* level.

RESULTS AND DISCUSSION

Synthesis of the nitro-carbazole OXEs

The five series of dyes have the same chromophore, namely a carbazole group. The syntheses of the different dyes are described in the Scheme 2. As the starting materials, we either used 9-ethyl-9H-carbazole (**1b**) which is commercially available or we synthesized 9-dodecyl-9H-carbazole (**1a**) with a very good yield (96%) by alkylation of carbazole with 1-bromododecane in the presence of a base. Once prepared, **1a** and **1b** were respectively converted as **2a** and **2b** by mean of Friedel-Crafts reactions using acetyl chloride or as **4a** and **4b** using butyryl chloride as the acylating agents. Purification of these compounds was done by column chromatography (SiO$_2$), enabling to separate the targeted compounds (*mono*-adduct) from the undesired *bis*-adducts. Then, nitration using nitric acid (65%) enabled to prepare **6a**, **6b**, **7a** and **7b** with reaction yields ranging from 78% to 88%. Noticeably, an alternative procedure was proposed for the synthesis of **6a**, **6b**, **7a** and **7b**, consisting first in the mono-nitration of **1a** and **1b**, providing **3a** and **3b** as solids. Notably, **3a** and **3b** could be recovered in pure form by a simple filtration of the precipitates and the two products could be obtained with reaction yields of 68% and 62% respectively. In a second step, Friedel-Crafts alkylation reactions with the appropriate acylating agent could provide **6a** and **6b** in 65 and 72% yield respectively. Here again, the two compounds could be obtained in pure form without any column chromatography. Carbaldehyde **5a** was prepared in 63% yield from 9-dodecyl-9H-carbazole (**1a**) by mean of a Vilsmeier Haack reaction using phosphoryl chloride (POCl$_3$) and DMF. Then, nitration of **5a** could provide **8a** in 72% yield. Once the different ketones or aldehydes were obtained, the different oximes **B10**, **C10**, **D10**, **E10** and **F10** could be prepared in excellent yields of about 90% using hydroxylamine hydrochloride and sodium acetate in a mixture of three solvents (THF/MeOH/H$_2$O). The final step consisted in converting the different oximes as oxime-esters by reaction with different acid chlorides in the presence of a base (triethylamine). The different reaction yields are given in the Table 1. Interestingly, the different oxime esters could be obtained in good yields ranging from 60% for **D9** to 94% for **B2**. It has to be noticed that the reaction yields are less good for the series D, E and F than for the series B and C. These lower yields are assigned to the presence of the

dodecyl chain providing an improved solubility to the different oxime esters and rendering the precipitation more difficult. As a result of this, part of the product was lost during the precipitation step. Detailed synthetic procedures giving access to the different dyes reported in this work are given in ESI.
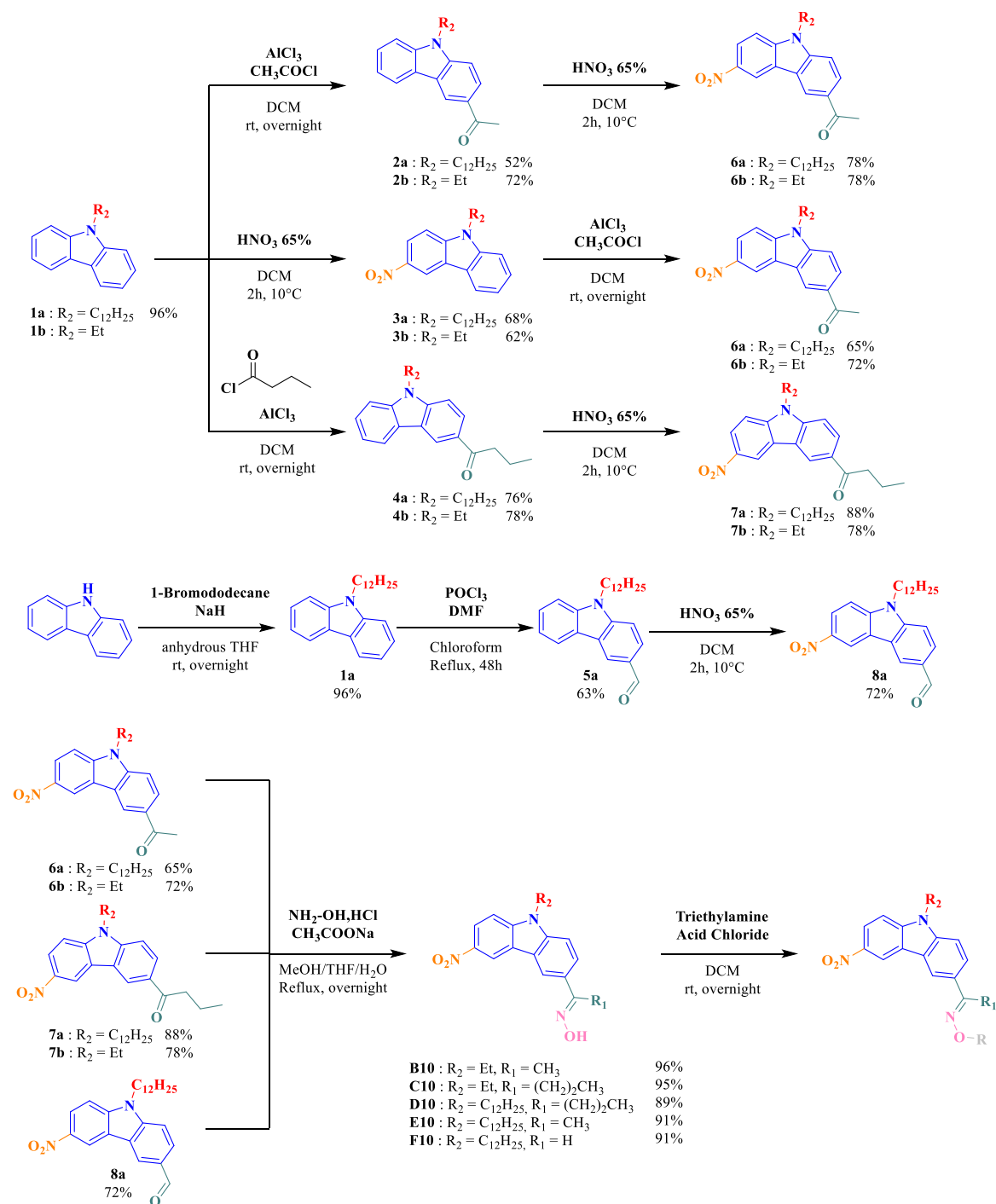
Scheme 2. Synthetic routes to the different OXEs.

Table 1. Yields of the different OXEs.

PI	B1	B2	B3	B4	B5	B6	B7	B8	B9	B10
Yield (%)	78	94	85	75	69	81	81	83	88	96
PI	C1	C2	C3	C4	C5	C6	C7	C8	C9	C10
Yield (%)	90	73	83	88	86	82	78	92	81	95
PI	D1	D2	D3	D4	D5	D6	D7	D8	D9	D10
Yield (%)	71	69	74	65	68	64	66	63	60	89
PI	E1	E2	E3	E4	E5	E6	E7	E8	E9	E10
Yield (%)	71	74	76	72	69	70	67	66	65	91
PI	F1	F2	F3	F4	F5	F6	F7	F8	F9	F10
Yield (%)	76	78	73	70	72	67	69	75	74	91

Light absorption properties

UV-visible absorption spectra of OXEs are shown in Figure 1 and the light absorption properties of different OXEs with interesting structures are listed in Table 2. All the OXEs demonstrated wide light absorption bands up to 440 nm. Specifically, λ_{max} of OXEs based on Series D was 372 nm. Compared to the compound **D10** without the oxime-ester functionality, λ_{max} of OXEs based on Series D were blue-shifted and the molar extinction coefficients at maximum absorption wavelength (ε_{max}) were increased. ε_{max} of **D1** and **D2** were 13000 and 14000 $M^{-1}cm^{-1}$ respectively. Furthermore, the molar extinction coefficients at 405 nm ($\varepsilon_{405\ nm}$) of all the OXEs were favorable (i.e., ε_{405nm} (**D1**) = 5200 $M^{-1}cm^{-1}$, ε_{405nm} (**D2**) = 5400 $M^{-1}cm^{-1}$), which was a perquisite for OXEs to be sensitive to the LED@405 nm as the irradiation source.
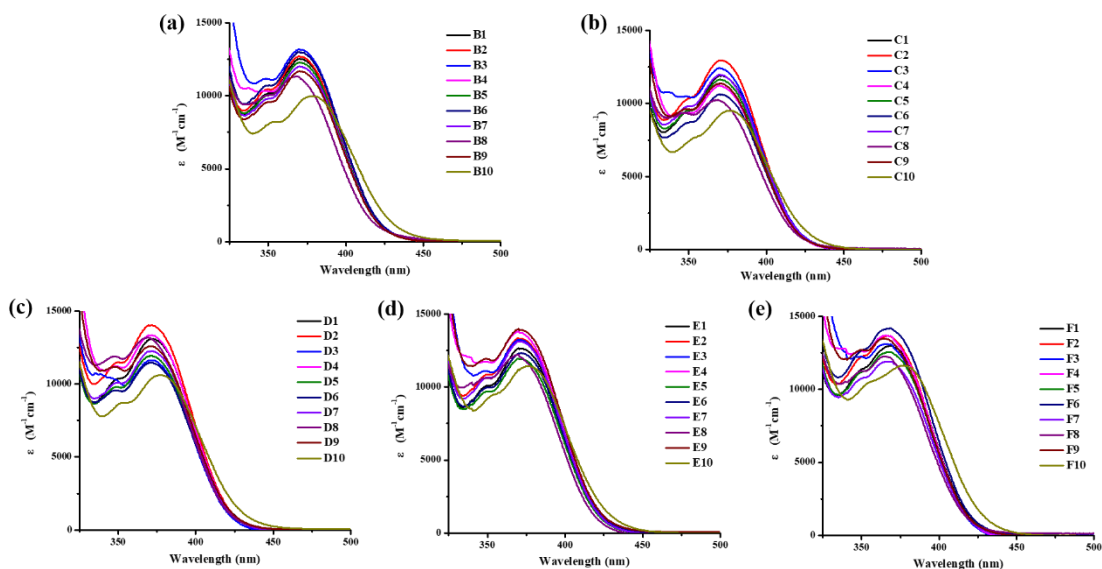
Figure 1. UV-visible absorption spectra of oxime ester derivatives in acetonitrile (a) OXEs based on Series B; (b) OXEs based on Series C; (c) OXEs based on Series D; (d) OXEs based on Series E; (e) OXEs based on Series F.

Table 2. Light absorption properties of some OXEs.

PI	λ_{max} (nm)	ε_{max} (M^{-1}cm^{-1})	$\varepsilon_{405\ nm}$ (M^{-1}cm^{-1})
B1	371	12500	4800
B2	371	12700	4700
C1	370	11900	4500
C2	370	12900	4600
D1	372	13000	5200
D2	372	14000	5400
E1	370	12700	5000
E2	370	13300	5100
F1	370	13000	4300
F2	370	13500	4200

Photochemical Mechanisms of OXEs

To study the photochemical mechanisms of OXEs, steady state photolysis of OXEs was performed upon exposure to LED@405 nm. Steady state photolysis of **D1** is illustrated in Figure 2 and the steady state photolysis of **D2** is given in Figure S1. With the increase of the irradiation time, the absorbance intensity of **D1** at λ_{max} = 372

nm declined gradually and the maximum absorption wavelength exhibited a red-shift, which could be attributed to the cleavage of N−O bond in **D1** structure. Indeed, after the cleavage of N−O bond, there was no photodegradation for nitro-carbazole chromophore attached with iminyl radical, and as a result, a modest decline of the absorbance intensity of **D1** at the maximum absorption wavelength was observed after irradiation.
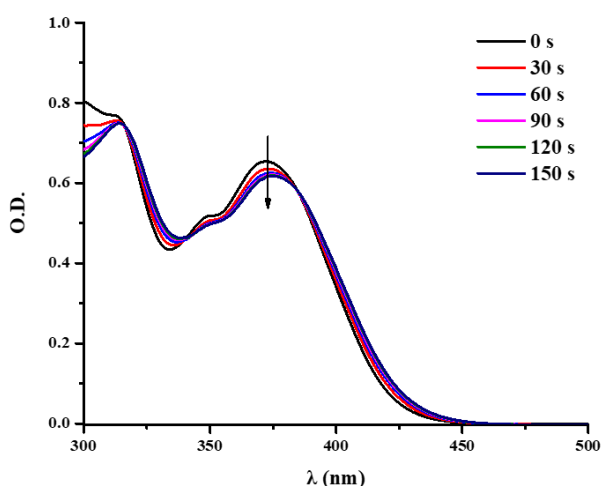

Figure 2. Steady state photolysis of **D1** in acetonitrile under LED@405 nm irradiation.

As illustrated in Figure 3a, the singlet excited state energy (E_{S1}) of **D1** was obtained from the crossing point of the UV-visible absorption and fluorescence emission spectra. The detection of singlet excited state energies for other OXEs are given in Figure S2. Enthalpies of the cleavage process for N−O bond ($\Delta H_{cleavage\ S1/T1} =$ BDE(N−O) – E_{S1}/E_T) from singlet state (S_1) or triplet state (T_1) were calculated,[14] which can be used to determine the favorability of the cleavage reactions. Parameters of some interesting structures are given in Table 3. All the values $\Delta H_{cleavage\ S1} < 0$ indicated that the cleavage of the N−O bond from the singlet state was energetically favorable. Furthermore, fluorescence lifetime of **D1** and other OXEs was measured (See Figure 3b and Figure S3). Fluorescence lifetimes for both OXEs (i.e., **D1** and **D2**) and the compounds (i.e., **D10**) without the oxime-ester functionality are shorter than the response time of the apparatus (1.4 ns). Therefore, such a short lifetime is an

intrinsic property for nitro-carbazole oxime chromophore. In addition, enthalpies of the cleavage process from T_1 were also favorable, which suggested that the cleavage process for N−O bond from T_1 cannot be ruled out. Based on the above results, the proposed photoinitiation mechanism of OXEs in this study is shown in Scheme 3. The OXEs transited from their ground states to their excited states upon light exposure, then the N−O bond dissociated to generate the iminyl and acyloxy radicals (reaction 1). Afterwards, the acyloxy radical underwent a decarboxylation to produce the active free radical $M^\bullet$ which can induce the polymerization of monomers (reaction 2).
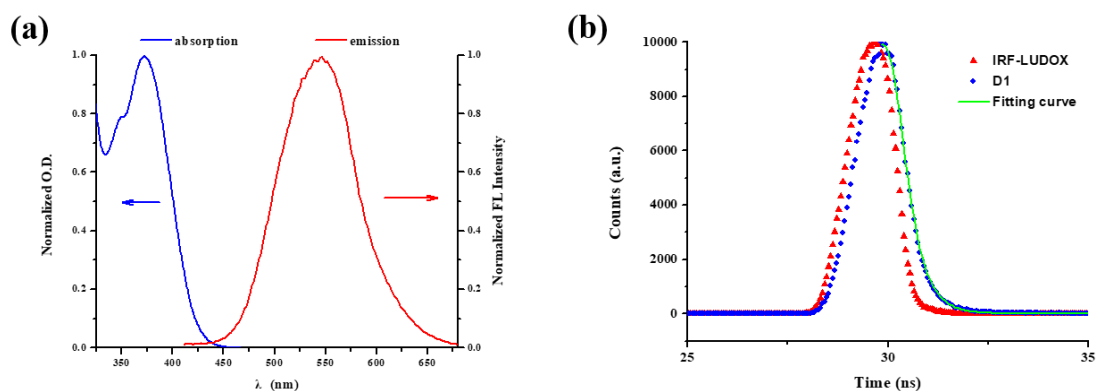
Figure 3. (a) Singlet state energy determination of D1; (b) Fluorescence decay curve of D1.

Table 3. Some parameters of the interesting OXEs.

PIs	N−O BDE (kcal mol^{-1})	E_{S1} (kcal mol^{-1})	$\Delta H_{\text{cleavage S1}}$ (kcal mol^{-1})	E_T (kcal mol^{-1})	$\Delta H_{\text{cleavage T1}}$ (kcal mol^{-1})
B1	44.16	64.98	-20.73	58.19	-14.03
B2	44.15	64.55	-20.40	58.11	-13.96
C1	44.98	65.65	-20.67	58.21	-13.23
C2	44.59	65.58	-20.99	58.11	-13.52
D1	45.03	65.21	-20.18	58.25	-13.22
D2	44.60	65.58	-20.98	58.18	-13.58
E1	44.61	68.24	-23.63	58.24	-13.63
E2	44.16	65.14	-20.98	58.14	-13.98
F1	46.21	65.89	-19.68	58.12	-11.91

F2	45.56	66.50	-20.94	58.31	-12.75
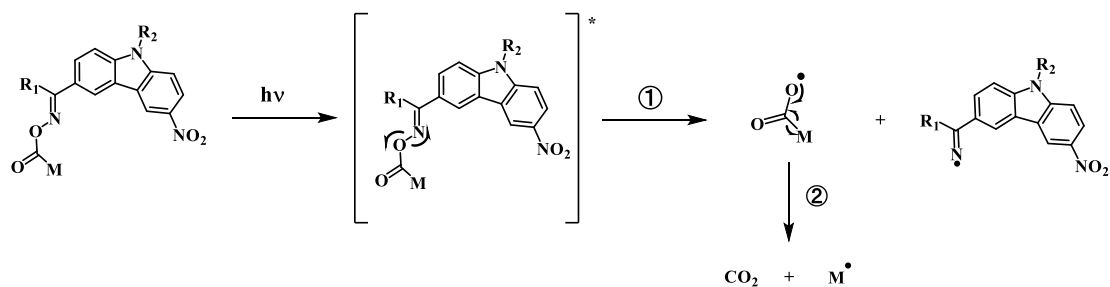
Scheme 3. Proposed photochemical mechanism of oxime ester PIs.

Free Radical Photopolymerization

Photoinitiation abilities of the investigated OXEs for the polymerization of TMPTA upon exposure LED@405 nm were studied using RT-FTIR. Polymerization profiles of TMPTA in the presence of OXEs are depicted in Figure 4. The final function conversions (FCs) and the polymerization rate of TMPTA are presented in Table 4. Specifically, the compounds **B10**, **C10**, **D10**, **E10**, and **F10** exhibited poor photoinitiation performance due to the absence of oxime-ester group. Interestingly, the compounds with the methyl substituent on oxime ester group (**B1**, **C1**, **D1**, **E1**, and **F1**) demonstrated the best photoinitiation ability in their respective series. As shown in the Figure 4f, a little higher FCs and polymerization rates were found in the presence of **C1**, **D1**, and **F1** than those with the well-known commercial photoinitiator TPO (see Table 4). Photopolymerization of monomers was also influenced by the concentrations of the PI. As shown in the Figure S4, the final function conversion of TMPTA became increasingly high with the increased concentration of **D1**. Indeed, the high concentration of PI can generate more free radicals to induce the polymerization. Moreover, those OXEs exhibited favorable performances in polymerization of thick samples (See Figure S5).
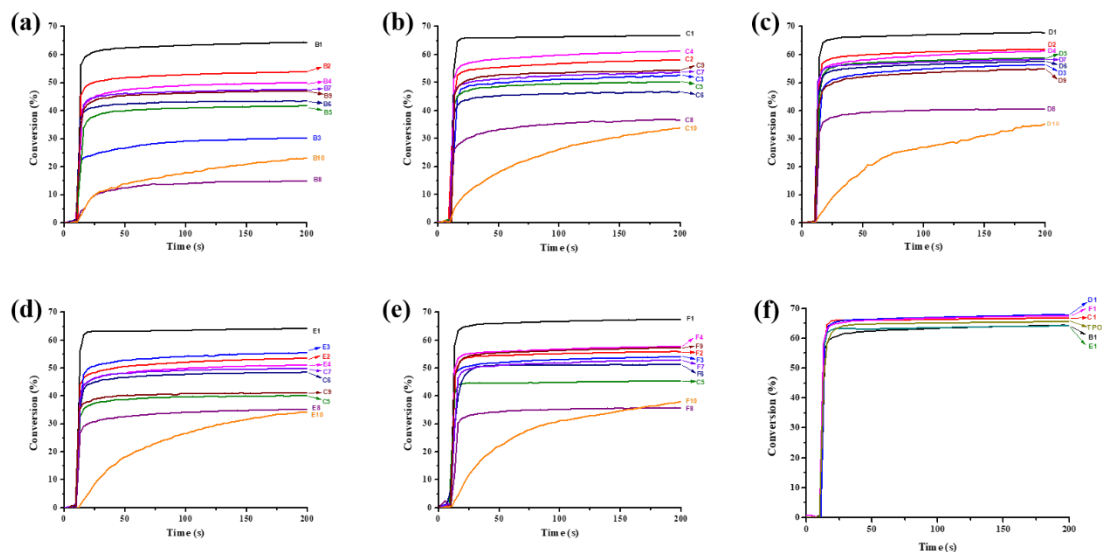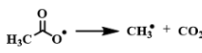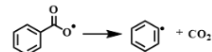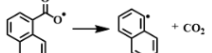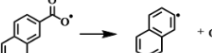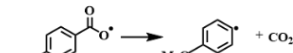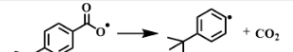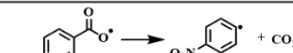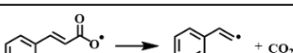
Figure 4. Photopolymerization profiles of TMPTA in laminate (~25 μm) upon exposure to LED@405 nm in the presence of photoinitiators (2×10^{-5} mol/g TMPTA) (a) OXEs based on Series B; (b) OXEs based on Series C; (c) OXEs based on Series D; (e) OXEs based on Series E; (e) OXEs based on Series F; (f) **B1**, **C1**, **D1**, **E1**, **F1** and TPO. The irradiation starts at t = 10 s.

Table 4. The final function conversions (FCs) and the maximum polymerization rate (Rp) of TMPTA in the presence of OXEs.

PIs	FC (%)	$R_p/[M]_0\times100$ (s^{-1})
B1	64	18.6
B2	54	15.0
C1	67	18.2
C2	58	14.5
D1	68	19.3
D2	62	14.6
E1	64	18.2
E2	53	14.2
F1	68	19.4
F2	56	12.0
TPO	66	15.4

Decarboxylation Reaction

All the OXEs demonstrated rather similar light absorption properties. It was interesting to explore the reason why OXEs with methyl substituent on oxime ester group exhibited the best photoinitiation ability among the studied compounds bearing other substituents. Decarboxylation is an important process for OXEs acting as photoinitiators. As reported, the generation of CO_2 was detected through the color response of solutions which can confirm the existence of decarboxylation.[13, 32] In our previous study, we reported the enthalpy for decarboxylation reactions ($\Delta H_{decarboxylation}$).[29] As given in Scheme 4, a $\Delta H_{decarboxylation}$ = - 4.94 kcal mol^{-1} was determined for the decarboxylation reaction of acetoxyl group, while $\Delta H_{decarboxylation}$ > 0 kcal mol^{-1} was found for the other compounds with benzoyloxy or acryloyloxy group. It indicated that the decarboxylation reaction for **D1** occurred more favorably than that for **D2-D9**. The simulated calculations proved the high reactivity of OXEs with methyl substituent theoretically.

Decarboxylation reactions	$\Delta H_{decarboxylation}$ (kcal mol^{-1})
H_3C—COO• ⟶ $CH_3^•$ + CO_2	-4.94
(benzoyloxy radical) ⟶ (phenyl radical) + CO_2	5.92
(naphthoyloxy radical) ⟶ (naphthyl radical) + CO_2	4.36
(naphthoyloxy radical) ⟶ (naphthyl radical) + CO_2	6.24
(methylbenzoyloxy radical) ⟶ (tolyl radical) + CO_2	6.92
MeO—(benzoyloxy radical) ⟶ MeO—(aryl radical) + CO_2	8.77
(tert-butylbenzoyloxy radical) ⟶ (aryl radical) + CO_2	6.97
O_2N—(benzoyloxy radical) ⟶ O_2N—(aryl radical) + CO_2	3.14
(cinnamoyloxy radical) ⟶ (styryl radical) + CO_2	7.64

Scheme 4. Enthalpies for the decarboxylation reactions ($\Delta H_{decarboxylation}$).[29]

In the present study, we further investigated the decarboxylation reaction in detail by monitoring the generation of CO_2 and detecting the produced radicals. CO_2 can be detected during the photopolymerization experiments using RT-FTIR. As shown in Figure 5a, in the **D1**/TMPTA system, it was found that a new absorption peak in infrared spectra at 2337 cm^{-1} appeared during photopolymerization which can be assigned to CO_2.[34, 35] More interestingly, the phenomenon was observed in other OXE/TMPTA systems but not in **D10**/TMPTA and TPO/TMPTA (see Figure S6), which can be the direct evidence that confirms the decarboxylation reaction for OXEs. In addition, the curve of absorption intensity (absorbance *vs* irradiation time) of CO_2 was presented for the first time. As illustrated in Figure 5b, between 10 s to 16 s, the acrylate function conversion increased rapidly accompanied by the generation of CO_2 in decarboxylation reaction (Line 1 and Line 3). The generation of CO_2 almost stopped at 16 s, and the polymerization was also almost completed at the same time. The same condition was also found in **D2**/TMPTA system (Line 2 and Line 4). Meanwhile, absorbance intensity of CO_2 for **D1**/TMPTA system was higher than in the **D2**/TMPTA system (Line 3 and Line 4) which demonstrated the decarboxylation reaction for **D1** more reactive than **D2**. In addition, the trend was also observed in other series OXEs (i.e., **B1**/TMPTA and **B2**/TMPTA systems) (see Figure S7), which was in full agreement with the simulated values of $\Delta H_{decarboxylation}$ (see Scheme 4). Absorbance of CO_2 declined gradually after 16 s due to its diffusion from the samples to the air.
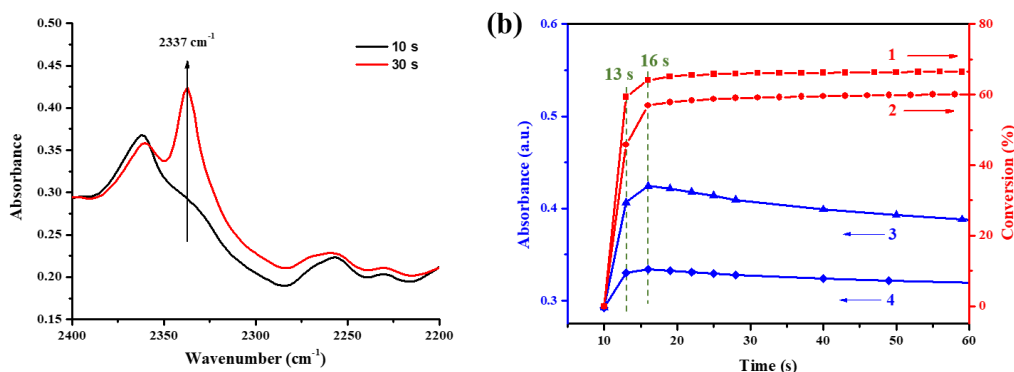
Figure 5. (a) Infrared spectra of **D1**/TMPTA in photopolymerization experiments at t =10 s and 30 s. (b) Line 1: Photopolymerization profiles (acrylate function conversion vs. irradiation time) of **D1**/TMPTA system; Line 2: Photopolymerization profiles (acrylate function conversion vs. irradiation time) of **D2**/TMPTA system; Line 3: The curve of absorption intensity (absorbance *vs* irradiation time) of CO_2 obtained from **D1**/TMPTA system; Line 4: The curve of absorption intensity (absorbance *vs.* irradiation time) of CO_2 obtained from **D2**/TMPTA system.

Besides CO_2, the generated radical was another product in the decarboxylation reactions. As shown in Figure 6a, two kinds of radicals were trapped by PBN in **D1** system after 5 s irradiation. Values of the hyperfine coupling constants for one radical adduct (75.7%) were $\alpha_N = 13.43$ G and $\alpha_H = 1.83$ G which can be assigned to the acetoxy radical ($CH_3COO^\bullet$).[36] The N−O bond in **D1** structures cleaved under irradiation and the formation of acyloxy radical was confirmed (reaction 1, Scheme 3). Another one (24.3%) with hyperfine coupling constants $\alpha_N = 14.64$ G and $\alpha_H = 3.70$ G could be assigned to methyl radical.[37] A portion of acetoxy radical decomposed into CO_2 and methyl radical after the decarboxylation (reaction 2, Scheme 3). It should be noted that only one radical was observed in **D2** (see Figure 6b) after 5 s irradiation. Values of the hyperfine coupling constants were $\alpha_N = 13.18$ G and $\alpha_H = 1.53$ G which can be assigned to the benzoyloxy radical ($C_6H_5COO^\bullet$).[37] The phenyl radical could not be found in **D2** system, which suggested that **D2** did not undergo any decarboxylation in solution. It indicated that the decarboxylation was more difficult to occur for **D2**, which corresponded to the results of related polymerization efficiency and the detection of CO_2 (see Figure 5).
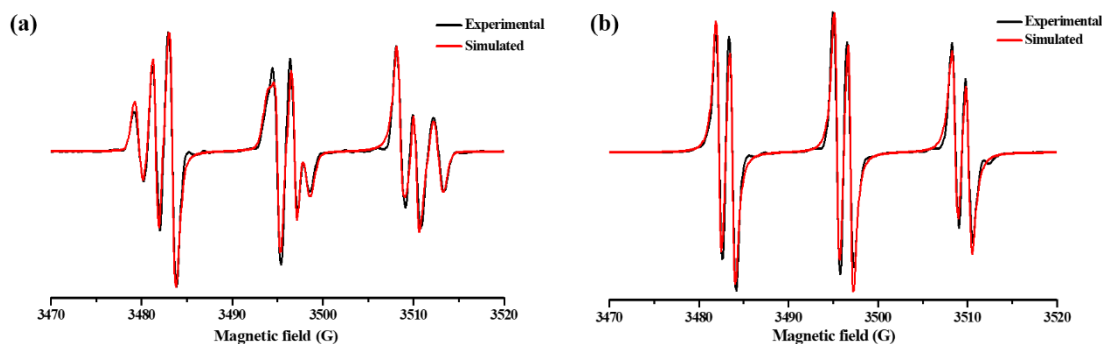
Figure 6. ESR-ST spectra of the radical adducts for (a) D1 and (b) D2 under LED@405 nm irradiation in *tert*-butylbenzene.

Chemical Structures/Photoinitiation Ability Relationship

Substituents R_1 and R_2 (see Scheme 1) introduced onto the chromophore exhibited only a slight influence on the intrinsic properties (light absorption, fluorescence lifetime, singlet excited state energy, and triplet state energy) of OXEs. The long alkyl chain of substituents (i.e., $R_2 = C_{12}H_{25}$) was only beneficial for the solubility of OXEs in monomers. The substituent R on oxime group can make a considerable impact on the decarboxylation reaction where the active free radicals were generated. The acetoxy can undergo a favorable decarboxylation process resulting in excellent photoinitiation abilities for **B1**, **C1**, **D1**, **E1**, and **F1**. In addition, **B8**, **C8**, **D8**, **E8** and **F8** demonstrated poor performance relatively. Nitro is a characteristic electron withdrawing group which could diminish the activity of the produced nitrobenzene radicals.

3D printing

Due to the good photoinitiation performance in the polymerization process, **D1**/TMPTA system was a reference system to carry out the direct laser write (DLW) and 3D printing experiments. **D1** was selected as a representative oxime ester exhibiting a high efficiency @405 nm (see Figure 4f). As shown in Figure 7a, the letter pattern "ET" (thickness ~1600 μm) was obtained through DLW within a short time (~ 2 min). The letter pattern demonstrated a high spatial resolution under the numerical optical

microscope. In addition, according to the computer model (see Figure 7b), 3D objects (thickness ~2 mm) were fabricated successfully using a stereolithography 3D printer (see Figure 7c).
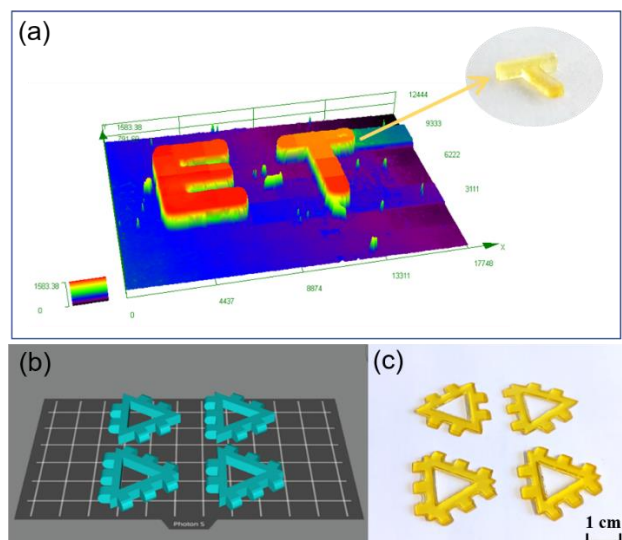

Figure 7. (a) The letter pattern observed by numerical optical microscope; (b) and (c) the computer model and the 3D printed objects.

Thermal Polymerization

OXEs can also generate free radicals through thermal degradation. DSC curves (Temperature *vs* Heat flow) of **B1**, **C1** and **D1** in TMPTA are presented in Figure 8a. The initial temperature of thermal polymerization ($T_{initial}$) and the temperature of maximun polymerization rate (T_{max}) as well as the final acrylate conversions (FC) of TMPTA are given in Table 5. $T_{initial}$ of them were all below 100 °C. As shown in Figure 8b, the liquid formulation of **D1**/TMPTA turned into a solid polymer when it was heated for 30 min at 130 °C. Interestingly, **B1**, **C1**, and **D1** demonstrated the dual photo/thermal initiator behavior. Other reported OXEs reported by us have demonstrated the potential application in many fields such as the preparation of carbon fiber composites for dual light/thermal activation.[27]
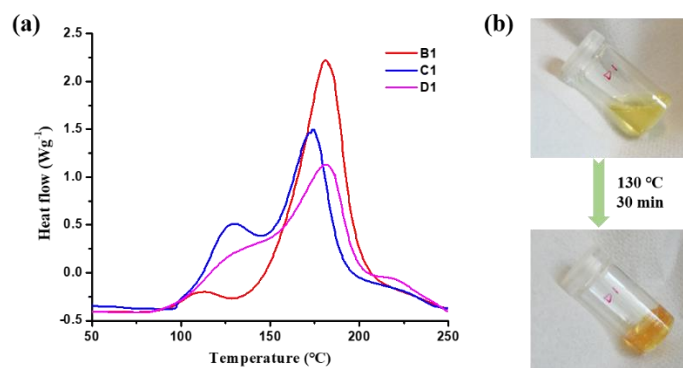
Figure 8. (a) DSC curves of OXEs in TMPTA; (b) the thermal polymerization of TMPTA in the presence of **D1**.

Table 5. Some parameters about thermal polymerization.

PIs	$T_{initial}$ (°C)	T_{max} (°C)	FC (%)
B1	83	181	68.0
C1	97	174	67.9
D1	82	182	70.7

Conclusions

A series of 50 OXEs (48 never synthesized before) bearing various substituents (R1 and R2) attached to the carbazole chromophore and different substituents (R) on the oxime group were designed and synthesized. These OXEs exhibited good light absorption properties in the near UV and visible region due to the presence of the nitro group on the carbazole scaffold. Photoinitiation abilities of OXEs in TMPTA were evaluated upon exposure to LED@405 nm. Some OXEs demonstrated better performance than the well-known commercial photoinitiator TPO. Notably, the high photoinitiation ability of **D1** allowed the fabrication of 3D objects using 3D printing technology. In addition, dual photo/thermal behavior was also observed for these OXEs. Investigation of the photochemical mechanism of OXEs showed that the N−O bond dissociated under irradiation could generate iminyl and acyloxy radicals. Then, the acyloxy radicals underwent a decarboxylation to decompose into CO_2 and active radicals which can induce the polymerization of monomers. The chemical structure-

photoinitiation ability relationship was also discussed. Specifically, the substituents R_1 and R_2 on chromophores barely changed the intrinsic properties of OXEs. In addition, it was found that the substituents (R) on the oxime group had the crucial effect on the photoinitiation ability of OXEs. Based on the simulated calculations reported previously, it was elaborated that the decarboxylation reaction can be investigated through the detection of CO_2 using the RT-FTIR and radicals using the ESR technique. This work confirmed the significance of decarboxylation reaction to photoinitiation ability and provided an achievable strategy for the design of novel and high-performance oxime ester-based photoinitiators.

Acknowledgements

Conflict of Interest

The authors declare no conflict of interest.

References

[1] Yagci Y, Jockusch S, Turro NJ. Photoinitiated Polymerization: Advances, Challenges, and Opportunities. Macromolecules 2010;43:6245-60.

[2] Zhang Y, Xu Y, Simon-Masseron A, Lalevée J. Radical photoinitiation with LEDs and applications in the 3D printing of composites. Chemical Society Reviews 2021;50:3824-41.

[3] Song HB, Baranek A, Worrell BT, Cook WD, Bowman CN. Photopolymerized Triazole-Based Glassy Polymer Networks with Superior Tensile Toughness. Advanced Functional Materials 2018;28:1801095.

[4] Corrigan N, Yeow J, Judzewitsch P, Xu J, Boyer C. Seeing the Light: Advancing Materials Chemistry through Photopolymerization. Angewandte Chemie International Edition 2019;58:5170-89.

[5] Dadashi-Silab S, Doran S, Yagci Y. Photoinduced Electron Transfer Reactions for Macromolecular Syntheses. Chemical Reviews 2016;116:10212-75.

[6] Regehly M, Garmshausen Y, Reuter M, König NF, Israel E, Kelly DP, et al. Xolography for linear volumetric 3D printing. Nature 2020;588:620-4.

[7] Al Mousawi A, Dumur F, Garra P, Toufaily J, Hamieh T, Graff B, et al. Carbazole Scaffold Based Photoinitiator/Photoredox Catalysts: Toward New High Performance Photoinitiating Systems and Application in LED Projector 3D Printing Resins. Macromolecules 2017;50:2747-58.

[8] Liu S, Brunel D, Sun K, Xu Y, Morlet-Savary F, Graff B, et al. A monocomponent bifunctional benzophenone–carbazole type II photoinitiator for LED photoinitiating systems. Polymer Chemistry 2020;11:3551-6.

[9] Tasdelen MA, Lalevée J, Yagci Y. Photoinduced free radical promoted cationic polymerization 40 years after its discovery. Polymer Chemistry 2020;11:1111-21.

[10] Zhang Y, Gao Y, Josien L, Nouali H, Vaulot C, Simon-Masseron A, et al. Photopolymerization of Zeolite Filler-Based Composites for Potential 3D Printing Application and Gas Adsorption Applications. Advanced Materials Technologies 2021;n/a:2100869.

[11] Xiao P, Zhang J, Dumur F, Tehfe MA, Morlet-Savary F, Graff B, et al. Visible light sensitive photoinitiating systems: Recent progress in cationic and radical photopolymerization reactions under soft conditions. Progress in Polymer Science 2015;41:32-66.

[12] Chen H, Noirbent G, Liu S, Brunel D, Graff B, Gigmes D, et al. Bis-chalcone derivatives derived from natural products as near-UV/visible light sensitive photoinitiators for 3D/4D printing. Materials Chemistry Frontiers 2021;5:901-16.

[13] Li Z, Zou X, Zhu G, Liu X, Liu R. Coumarin-Based Oxime Esters: Photobleachable and Versatile Unimolecular Initiators for Acrylate and Thiol-Based Click Photopolymerization under Visible Light-Emitting Diode Light Irradiation. ACS Applied Materials & Interfaces 2018;10:16113-23.

[14] Dietlin C, Trinh TT, Schweizer S, Graff B, Morlet-Savary F, Noirot P-A, et al. Rational Design of Acyldiphenylphosphine Oxides as Photoinitiators of Radical Polymerization. Macromolecules 2019;52:7886-93.

[15] Strużyńska-Piron I, Loccufier J, Vanmaele L, Vankelecom IFJ. Parameter Study on the Preparation of UV Depth-Cured Chemically Resistant Polysulfone-Based Membranes. Macromolecular Chemistry and Physics 2014;215:614-23.

[16] Dietliker K, Jung T, Benkhoff J, Kura H, Matsumoto A, Oka H, et al. New Developments in Photoinitiators. Macromolecular Symposia 2004;217:77-98.

[17] Mallavia R, Sastre R, Amat-Guerri F. Photofragmentation and photoisomerization of O-acyl-

α-oxooximes: Quantum yields and mechanism. Journal of Photochemistry and Photobiology A: Chemistry 2001;138:193-201.

[18] Xu J, Ma G, Wang K, Gu J, Jiang S, Nie J. Synthesis and photopolymerization kinetics of oxime ester photoinitiators. Journal of Applied Polymer Science 2012;123:725-31.

[19] Li Z, Zou X, Shi F, Liu R, Yagci Y. Highly efficient dandelion-like near-infrared light photoinitiator for free radical and thiol-ene photopolymerizations. Nature Communications 2019;10:3560.

[20] Dietliker K, Hüsler R, Birbaum JL, Ilg S, Villeneuve S, Studer K, et al. Advancements in photoinitiators—Opening up new applications for radiation curing. Progress in Organic Coatings 2007;58:146-57.

[21] Dworak C, Liska R. Alternative initiators for bimolecular photoinitiating systems. Journal of Polymer Science Part A: Polymer Chemistry 2010;48:5865-71.

[22] Qiu W, Li M, Yang Y, Li Z, Dietliker K. Cleavable coumarin-based oxime esters with terminal heterocyclic moieties: photobleachable initiators for deep photocuring under visible LED light irradiation. Polymer Chemistry 2020;11:1356-63.

[23] Ma X, Gu R, Yu L, Han W, Li J, Li X, et al. Conjugated phenothiazine oxime esters as free radical photoinitiators. Polymer Chemistry 2017;8:6134-42.

[24] Qiu W, Zhu J, Dietliker K, Li Z. Polymerizable Oxime Esters: An Efficient Photoinitiator with Low Migration Ability for 3D Printing to Fabricate Luminescent Devices. ChemPhotoChem 2020;4:5296-303.

[25] Fast DE, Lauer A, Menzel JP, Kelterer A-M, Gescheidt G, Barner-Kowollik C. Wavelength-Dependent Photochemistry of Oxime Ester Photoinitiators. Macromolecules 2017;50:1815-23.

[26] Zhou R, Pan H, Wan D, Malval J-P, Jin M. Bicarbazole-based oxime esters as novel efficient photoinitiators for photopolymerization under UV-Vis LEDs. Progress in Organic Coatings 2021;157:106306.

[27] Liu S, Graff B, Xiao P, Dumur F, Lalevée J. Nitro-Carbazole Based Oxime Esters as Dual Photo/Thermal Initiators for 3D Printing and Composite Preparation. Macromolecular Rapid Communications 2021;42:2100207.

[28] Hammoud F, Lee Z-H, Graff B, Hijazi A, Lalevée J, Chen Y-C. Novel phenylamine-based oxime ester photoinitiators for LED-induced free radical, cationic, and hybrid polymerization. Journal of Polymer Science 2021;59:1711-23.

[29] Hammoud F, Giacoletto N, Noirbent G, Graff B, Hijazi A, Nechab M, et al. Substituent effects on the photoinitiation ability of coumarin-based oxime-ester photoinitiators for free radical photopolymerization. Materials Chemistry Frontiers 2021;5:8361-70.

[30] Wang W, Jin M, Pan H, Wan D. Phenylthioether thiophene-based oxime esters as novel photoinitiators for free radical photopolymerization under LED irradiation wavelength exposure. Progress in Organic Coatings 2021;151:106019.

[31] Chen S, Jin M, Malval J-P, Fu J, Morlet-Savary F, Pan H, et al. Substituted stilbene-based oxime esters used as highly reactive wavelength-dependent photoinitiators for LED photopolymerization. Polymer Chemistry 2019;10:6609-21.

[32] Zhou R, Sun X, Mhanna R, Malval J-P, Jin M, Pan H, et al. Wavelength-Dependent, Large-Amplitude Photoinitiating Reactivity within a Carbazole-Coumarin Fused Oxime Esters Series. ACS Applied Polymer Materials 2020;2:2077-85.

[33] McCurdy KG, Laidler KJ. THERMOCHEMICAL STUDIES OF SOME ACRYLATE AND

METHACRYLATE POLYMERIZATIONS IN EMULSION SYSTEMS. Canadian Journal of Chemistry 1964;42:818-24.

[34] Schultz CP, Eysel HH, Mantsch HH, Jackson M. Carbon Dioxide in Tissues, Cells, and Biological Fluids Detected by FTIR Spectroscopy. The Journal of Physical Chemistry 1996;100:6845-8.

[35] Kumar J, D'Souza SF. Preparation of PVA membrane for immobilization of GOD for glucose biosensor. Talanta 2008;75:183-8.

[36] Ding Y, Jiang S, Gao Y, Nie J, Du H, Sun F. Photochromic Polymers Based on Fluorophenyl Oxime Ester Photoinitiators as Photoswitchable Molecules. Macromolecules 2020;53:5701-10.

[37] Haire LD, Krygsman PH, Janzen EG, Oehler UM. Correlation of radical structure with EPR spin adduct parameters: utility of the proton, carbon-13, and nitrogen-14 hyperfine splitting constants of aminoxyl adducts of PBN-nitronyl-13C for three-parameter scatter plots. The Journal of Organic Chemistry 1988;53:4535-42.

TOC graphic: